Surface & Coatings Technology 263 (2015) 15–20

Contents lists available at ScienceDirect

Surface & Coatings Technology

journal homepage: www.elsevier.com/locate/surfcoat

The effect of chromium on the gamma to alpha phase transition of alumina coating formed on 316L SS by a cathodic micro arc deposition (CMAD) process

Cheng Zeng [a], Yunhan Ling [a,*], Shantong Li [a], Yongchu Rao [b], Yixiang Chen [c]

[a] Lab of Advanced Materials, School of Materials Sciences and Engineering, Tsinghua University, Beijing 100084, China
[b] China Academy of Engineering Physics, Mianyang 621900, China
[c] Technical Institute of Physics and Chemistry, Chinese Academy of Sciences, Beijing 100190, China

ARTICLE INFO

Article history:
Received 20 August 2014
Accepted in revised form 30 December 2014
Available online 6 January 2015

Keywords:
Al_2O_3
Cr_2O_3
Coating
Cathodic micro arc deposition (CMAD)
Phase transition

ABSTRACT

Alumina ceramic coatings are widely used because of their favorable physical and chemical stability. However, the formation of stable alpha phase alumina on metallic substrates at lower temperatures still presents technical challenges. In this work, an Cr doped Al_2O_3 ceramic coating was successfully fabricated on 316L stainless steel by a new cathodic micro-arc deposition (CMAD) technique using $Al(NO_3)_3$ as the precursor. We studied the effect of chromium on its phase transition from gamma to alpha as well as the underlying mechanism. Phase and chemical composition distribution, surface morphology, and photoluminescence data were characterized by X-ray diffraction (XRD), electron probe microanalysis (EPMA), a scanning electron microscope (SEM) with an energy dispersive spectroscopy (EDS), and a microscopic confocal Raman spectrometer (MCRS). The results showed that the ceramic coatings have a porous microstructure and were mainly composed of Cr doped α-Al_2O_3 and γ-Al_2O_3. This suggests that the introduction of Cr in the electrolyte solution can promote the nucleation and growth of the corundum phase of α-Al_2O_3. Based on the comparison of conventional heat treatment of alumina precipitates with and without Cr dopant via a sol–gel process, we proposed that the reducing atmosphere and local high sparking temperature that subsequently enhances the diffusion of defects in oxides may be contributed to this transition. This finding might provide a simple, cost efficient way to fabricate corundum alumina coatings on metallic substrates under mild temperatures without sacrifice of its mechanical properties.

1. Introduction

Alumina is one of the most important technical ceramics. Its mechanical, electrical, and optical properties enable a wide range of uses in microelectronics, catalysis, lasers, optics, and refractories. With a close-packed structure and large lattice energy, α-Al_2O_3 is the most stable phase in the family of aluminum oxides. It has a high melting temperature, high hardness and good chemical durability. Because of its favorable physical and chemical properties, α-Al_2O_3 is widely used in ceramics, refractory products, and chemical engineering [1–3]. More recently, α-Al_2O_3 was found to be an excellent candidate as a tritium permeation barrier, which is a critical blanket material in the International Thermonuclear Experimental Reactor (ITER) design [4].

Alumina ceramic coatings have widespread applications because of their physical and chemical stability. Although alumina is most regarded among the tritium permeation barriers [5–7], the formation of stable phase alpha alumina on metallic substrates at lower temperatures still faces technical challenges. Al_2O_3 exists in more than 15 distinct crystallographic phases, and can undergo a variety of transitions until it reaches the most thermodynamically stable corundum structure—α-Al_2O_3 [8]. Previous studies have reported that the phase transformation occurs at a high temperature (over 1000 °C) [9–11]. Nevertheless, high temperature environments always lead to the so-called sensitization effect which refers to the precipitation of carbides at grain boundaries in a stainless steel or alloy, causing the steel or alloy to be degraded in mechanical properties and/or to be susceptible to intergranular corrosion or intergranular stress corrosion cracking. Thus, a viable preparation of α-Al_2O_3 at 650–700 °C that does not affect the properties of the SS substrate is urgently needed. There are two ways to fabricate α-Al_2O_3 at low temperatures: the first activates the material surface with surface bombardment of high-energy ions [12,13], and the second introduces inductive dopants such as Cr_2O_3, F^- and Fe^{2+} to facilitate the formation of α-Al_2O_3 [14–17].

Recently, cathodic micro arc deposition (CMAD) has been shown to fabricate diamond-like carbon films and ceramic coatings on the substrates of metals and their alloys [18,19]. The CMAD process includes the precipitation of the precursor, pyrolysis of hydroxide, and the formation of the ceramic phase. The use of high-energy surface environments can significantly enhance the material properties of the surface

* Corresponding author. Tel.: +86 1062772856; fax: +86 1062772507.
E-mail address: yhling@mail.tsinghua.edu.cn (Y. Ling).

http://dx.doi.org/10.1016/j.surfcoat.2014.12.072
0257-8972/

without seriously affecting the substrate. Many attempts have been made to fabricate alumina ceramics on titanium or stainless steel substrate, and monolithic alumina coatings formed by CMAD have already been studied previously [20]. However, to the best of our knowledge, Cr doped Al_2O_3 ceramic coatings have not been reported.

This paper studies the phase composition of the CMAD layer obtained on the 316L stainless steel substrate. We found that the inclusion of Cr can promote the formation of stable phase Al_2O_3. The surface morphology, phase, and chemical composition were studied and the mechanism of chromium dopant effects was preliminarily investigated.

2. Experimental details

2.1. Alumina coating via CMAD

316L stainless steel with an EDS assay of 17 wt.% chromium was selected as the substrate and incised into sheets with dimensions of 20 mm × 10 mm × 1 mm by an electric sparking wire-cut. These were mechanically polished and thoroughly cleaned to serve as the cathode with graphite as the anode. The electrolytes employed in this work were $Al(NO_3)_3 \cdot 9H_2O$ (0.3 mol/L), $Cr(NO_3)_3 \cdot 9H_2O$ and ethanol (80 mL). The molar concentration of $Cr(NO_3)_3$ corresponds to the weight percentage ratio between Cr and $Al(NO_3)_3$ as 0.0%, 0.5%, 1.0%, and 1.5%, that is, if all of $Cr(NO_3)_3$ and $Al(NO)_3$ in the electrolyte precipitate and form a solid solution of Cr doped Al_2O_3, 0, 0.5%, 1% and 1.5wt.%Cr/$Al(NO_3)_3$ correspond to 0, 1.9%, 3.9% and 5.8 mol.%Cr_2O_3/Al_2O_3 respectively. The four samples will be defined henceforth as 0.0%Cr, 0.5%Cr, 1.0%Cr, and 1.5%Cr. An HSLM-20 power source was used for the CMAD process, which used a voltage of 360 V for 15 min in an ice bath.

The morphologies of the coatings were evaluated by field emission scanning electron microscopy (FESEM, JSM-7001F) with energy dispersive spectroscopy. The main elemental distribution along the cross section was measured by EPMA(JXA-8230) with a wavelength dispersive spectrometer (WDS) mode. The phase composition of the coatings was analyzed by X-ray diffraction (V2500) with Cu Kα radiation at a scanning speed of 8°/min with small angle grazing mode and fixed angle of 3°.

The photoluminescence was characterized with a confocal Raman spectrometer (RM2000/Renishaw Corporation, UK) to understand the mechanism of Cr inductive effects. This system used a 633-nm laser at room temperature. Raman mapping of the cross section occurred from 4000 cm^{-1} to 5000 cm^{-1} and used LabRAM HR Evolution software. The PL spectra used 532 nm excitation and wavelength from 675.8 nm to 724.8 nm with 35 data points in between.

Photoelectrochemical (PEC) measurements used a three-electrode cell to semi-quantitatively describe the defects in the coatings containing different amounts of Cr. The as-prepared samples acted as the working electrode, the platinum foil acted as the counter electrode, and the saturated calomel electrode (SCE) acted as the reference. Electrochemical signals were recorded with a universal electrochemical interface analyzer Zahner IM6e. A 100 mW/cm^2 Xenon arc lamp simulated solar light in the PEC measurement. Borate buffer with pH 8.0 was used as the electrolyte. The front surface of the working electrode was sealed by epoxy leaving an area of 0.4 cm^2.

2.2. Formation alumina powders via sol–gel process

To compare the dopant effect, alumina powders via sol–gel process were designed. The starting materials for hydrated alumina are $Al(NO_3)_3 \cdot 9H_2O$ and $Cr(NO_3)_3 \cdot 9H_2O$. These were dissolved into 80 mL of distilled water. Precursors of 0.0%Cr and 1.5%Cr were synthesized. Precursors were produced by dropping 25% (*v*/*v*) ammonia water (AW) into the solution at a low speed under magnetic stirring at room temperature. The resulting suspensions were aged for 12 h at room temperature, filtered with distilled water twice, rinsed another two times with ethyl alcohol and then dried at 100 °C for 10 h. After an intermediate grinding, the precursors were sintered at 600 °C, 900 °C, and 1000 °C for 4 h.

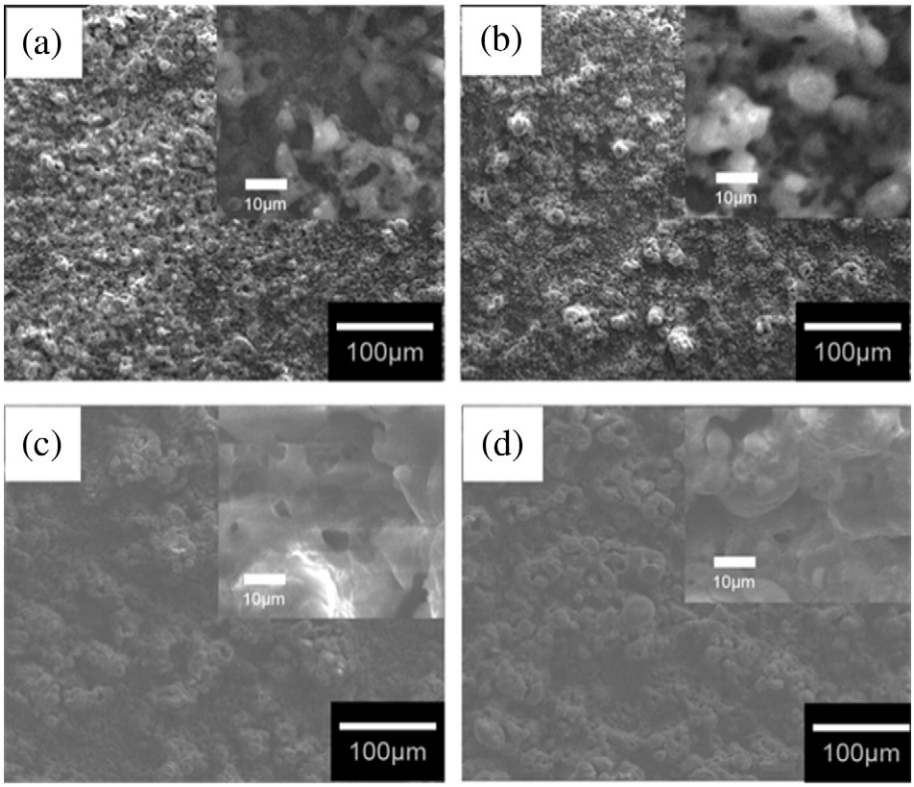

Fig. 1. Surface morphologies of ceramic coatings after 15 min of the CMAD process (a) 0.0%Cr, (b) 0.5%Cr, (c) 1.0%Cr, and (d) 1.5%Cr.

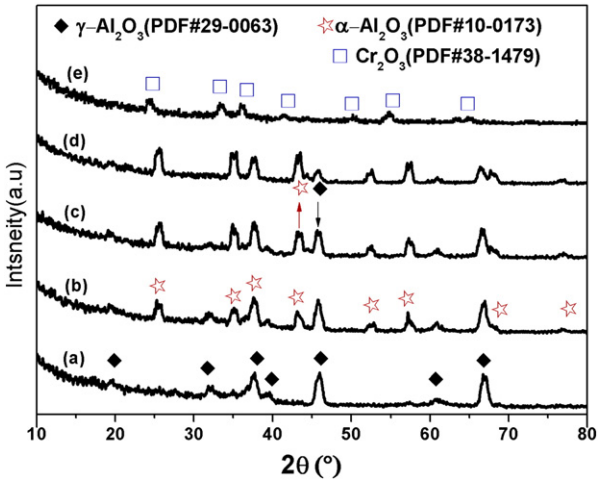

Fig. 2. X-ray diffraction patterns of the Al_2O_3 coatings with dopants of (a) 0.0%Cr, (b) 0.5%Cr, (c) 1.0%Cr, (d) 1.5%Cr, and (e) monolithic Cr_2O_3.

Phase identification of the precursors and the powders sintered at different temperatures was performed on D8 Advance X-ray diffractometer with a scanning speed of 6°/min in the $_{\theta-2\theta}$ scan mode. Differential scanning calorimetry (DSC) of the precursors after drying was made on a DSC analyzer (Mode STA449F3, NETZSCH) under argon with a heating rate of 10 °C/min between 25 °C and 1300 °C. Thermal gravimetric analysis (TG) used a TG analyzer.

3. Results and discussion

3.1. Morphology and phase analysis

The surface morphologies of the samples made with CMAD are shown in Fig. 1. It was clear that micron-sized particles were generated on the surface. The 1.5%Cr particles were much larger than 0.0%Cr sample. The samples were black except the 0.0%Cr, which was grey. The surface was coarse with a large number of irregular pores. The porous surface may come from the residual discharge channels. The EDS results showed that all samples are composed mainly of aluminum, oxygen and chromium. The four samples of 0.0%Cr, 0.5%Cr, 1.0%Cr, and 1.5%Cr (0, 1.9, 3.9 and 5.8 mol.%Cr_2O_3/Al_2O_3) have Cr weight fractions of ca. 2.3, 5.1, 7.2 and 12.6%. The Al is from the electrolyte, and Cr is from both the substrate and the solution.

X-ray diffraction spectra of the four treated samples are shown in Fig. 2. The coated samples mainly consist of α-Al_2O_3 and γ-Al_2O_3. The proportion of α-Al_2O_3 increased as a function of chromium in the electrolytes. Two peaks marked with arrows belong to α-Al_2O_3 ((113), red up arrow) and γ-Al_2O_3 ((400), black down arrow), respectively. These were used to estimate the transition proportion of α-Al_2O_3. Nearly 0%, 35%, 49% and 67% α-Al_2O_3 were obtained for samples of 0.0%Cr, 0.5%Cr, 1.0%Cr and 1.5%Cr.

The line scanning result is depicted in Fig. 3. The Al content varied with O content, which suggests that the coatings were predominately Al_2O_3. The thickness of the coatings in the 0.0%Cr and 1.5%Cr was approximately 80 μm, and a transitional layer close to the substrate surface may exist according to EPMA data. The chromium concentration in the coating is consistent with the amount introduced in the electrolytes for the 0.0%Cr and 1.5%Cr. EDS and EPMA results confirmed that Cr and Fe were incorporated into the coatings. Given the high energy of plasma, an inter diffusion cannot be avoided; thus Cr and Fe element were incorporated into the coatings. The EDS data showed that Fe concentrations of samples 0.0%Cr, 0.5%Cr, 1.0%Cr and 1.5%Cr are ca. 5.5, 1, 0.53, 0 wt.%, while the Cr concentration varies conversely.

3.2. Mechanism investigation

Chromium can significantly modulate the formation of α-Al_2O_3. The α-Al_2O_3 is very stable, but difficult to form at room temperature. We found that if the electrolyte merely consisted of $Cr(NO_3)_3$ (0.1 mol/L) and ethanol the coating has hexagonal chromic oxide eskolaite (XRD data; Fig. 2). This is the same crystal structure as α-Al_2O_3. However, as Fig. 2 shows, the individual diffraction spectra of eskolaite cannot be separated in the electrolytes of blending $Cr(NO_3)_3$ and $Al(NO_3)_3$. Consequently, chromium oxide diluted into the lattice of the aluminum oxide forms a solid solution. The elemental line scanning results were in agreement with the analysis and show that the coatings were mainly composed of Cr doped Al_2O_3.

Fig. 4 presents the PL spectra of the alumina coating sample contained 0.0%Cr and 1.5%Cr. A sharp, intense doublet, commonly labeled R_1 and R_2 at ~693 nm may be from Cr^{3+} ions in a high crystal-field environment under the distorted octahedral symmetry of ionic oxygen in α-Al_2O_3 [21]. As noted above, the chromium in the 0.0%Cr is

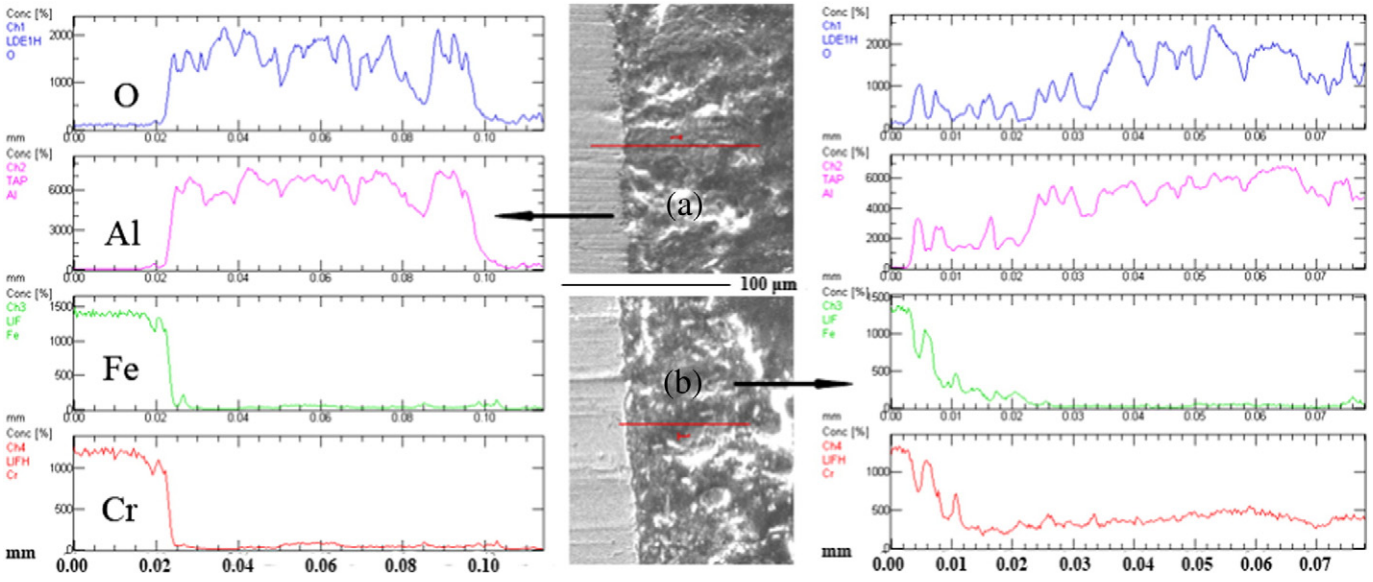

Fig. 3. EPMA elemental line scanning of the alumina coatings with Cr (a) 0.0% and (b) 1.5%.

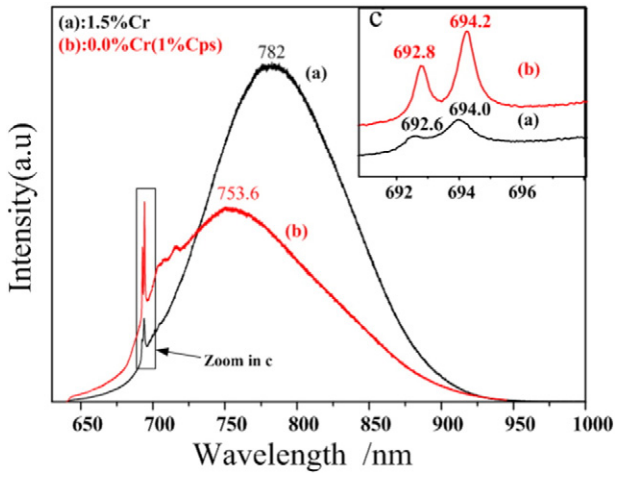

Fig. 4. PL spectra of the alumina coating with 0.0%Cr and 1.5%Cr.

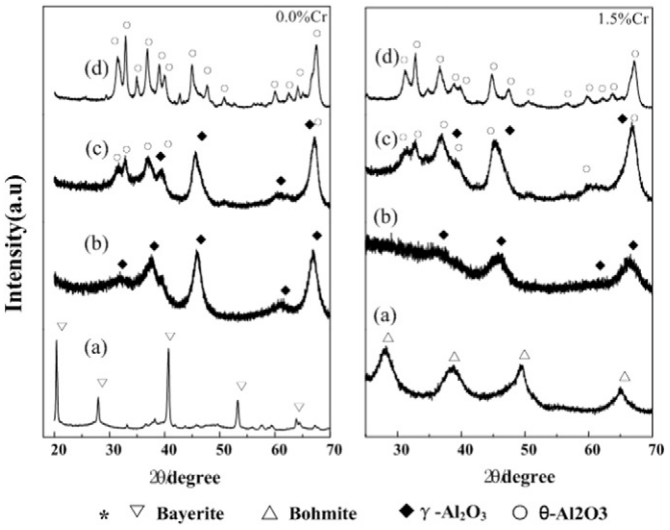

Fig. 6. XRD patterns of the alumina precursor powders calcined at (a) 100 °C, (b) 600 °C, (c) 900 °C, and (d) 1000 °C.

from the substrate. The luminescence intensity of 1.5%Cr was not as strong as that of 0.0%Cr because of the concentration quenching effect.

Judging from the luminescence spectra, chromium is doped into the lattice of α-Al_2O_3. The R-line of the 1.5%Cr sample showed a blue shift to that of 0.0%Cr. As reported previously, there is a positive correlation between the frequency of R-line and the Cr concentration in α-Al_2O_3 [22]. Therefore, it is reasonable to infer that the introduction of chromium in the electrolyte caused a concentration increase of chromium-doped α-Al_2O_3 on the surface. In addition, an intense and broad emission position can be distinguished at ~753.6 nm for the 0.0%Cr sample and ~782.0 nm for sample 1.5%Cr.

In contrast to the characteristic luminescence, the broad photoluminescence peak has a red shift as concentration increases. This broad transition results from the Cr^{3+} in a relatively low crystal-field environment, which is caused by a strong optical electronic states and lattice interaction according to the Huang-Rhys parameter [21,23]. Moreover, solid physics analysis explicitly indicates that the stronger the interaction, the lower the emissive frequency [21]. To give a rational explanation of the Cr doping effect, we conclude that the enhanced interaction with Cr doping contributes to a structure with more defects. To the best of our knowledge, the rate determining step in the formation of α-Al_2O_3 is the rearrangement of the oxygen ion. Thus, the largest activation free energy is needed during the anion migration. We conclude that the structure with more defects may result from the generation of more dislocations or point defects, like oxygen vacancies and chromium interstitial atoms. Given the larger number of defects in the lattice or at the interface between α-Al_2O_3 and γ-Al_2O_3, the activation energy is reduced because the oxygen ion rearranges more easily by means of these defects.

Raman mapping of the cross section showed that Cr doped α-Al_2O_3 was present in the entirety of both samples. The average total intensities of 0.0%Cr are much larger than that of 1.5%Cr. This was in agreement with the result of the PL spectra. The R_2 peak of 0.0%Cr was centered at ~4389 cm^{-1} (~694.06 nm) while 1.5%Cr at ~4384 cm^{-1} (~693.82 nm). This concurred with the PL data and indicates that there was more Cr in the α-Al_2O_3 of the 1.5%Cr sample than the 0.0%Cr one.

As mentioned in subsection 3.1, sample 0.0%Cr was grey while 1.5%Cr was black. Similarly, white titanium dioxide nanoparticles become black after hydrogen doping [24]. This suggests that Cr doping and the reductive environment introduced more localized defect states in the band gap of Al_2O_3, so that the energy levels of the excited electrons may decrease dramatically. To test the assumption that easier α-Al_2O_3 formation was due to the defects serving as a transformation shortcut, a transient photocurrent response was implemented at 0.8 V for an hour with three light cycles. Before testing, the open circuit potential was measured for 30 min to make the testing environment stable. The CMAD process for 0.0%Cr and 1.5%Cr samples was shortened to 5 min to obtain a current large enough to be measured. Similar XRD results and color phenomenon were seen at 5 min.

The PEC results are presented in Fig. 5. The total current of both samples was small, indicating that the resistance of both samples for

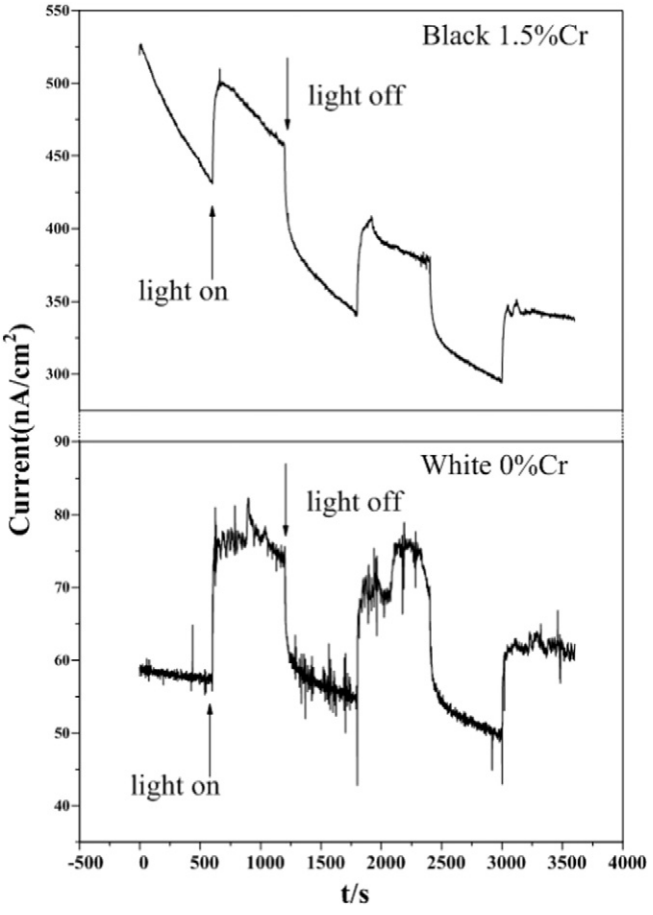

Fig. 5. Transient photocurrent response comparisons of alumina coatings with 0.0%Cr and 1.5%Cr.

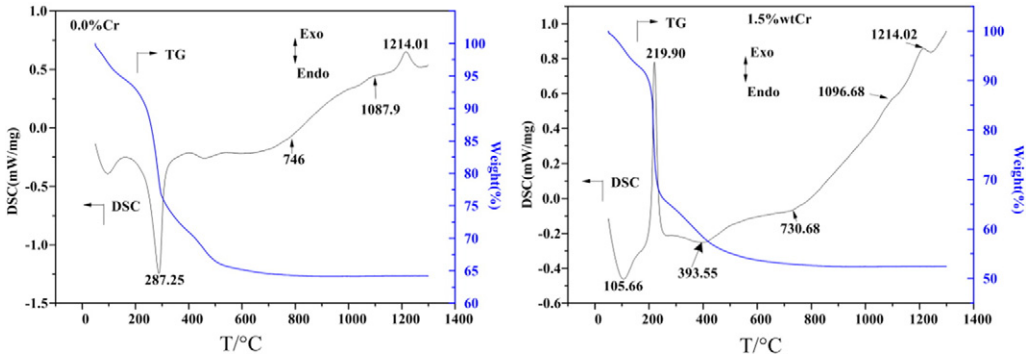

Fig. 7. DSC/TG curves of the alumina precursors doped with 0.0%Cr and 1.5%Cr.

only 5 min was large. The increasing current seen with the 0.0%Cr sample was about 15 nA and 60 nA for the 1.5%Cr a 3 fold increase. The results showed that more defects or lower energy levels arose in the Al_2O_3 coatings after the introduction of chromium. Indeed, pure alumina is an insulator with an energy band gap of 9.9 eV that cannot be activated by solar light. The structure with more defects therefore should play a significant role in the phase transition of Al_2O_3 during the CMAD process.

Compared to the CMAD technique, the sol–gel procedure produced powders at different sintering temperatures at the same concentration of chromium as the CMAD technique. The XRD results are summarized in Fig. 6 and elucidate that the aluminum oxide hydroxides are Bayerite for 0.0%Cr powder and Bohmite for 1.5%Cr powder. The precursors of the two samples followed the same polymorphic transformation before 1000 °C. It is generally accepted that the un-doped precursor undergoes the sub-adjacent series before the final conversion to the stable phase α-Al_2O_3 [25] as:

$$\textit{Bayerite or Bohmite} \rightarrow \gamma\text{-}Al_2O_3 \rightarrow \delta\text{-}Al_2O_3 \rightarrow \theta\text{-}Al_2O_3 \rightarrow \alpha\text{-}Al_2O_3$$

The transient phase of δ-Al_2O_3 cannot be distinguished in our work because the transformation of δ-Al_2O_3 to θ-Al_2O_3 is already completed at 900 °C, but the thermodynamically stable phase of α-Al_2O_3 was not present even up to 1000 °C.

The DSC/TG curves of the two dried precursors made from the AW precipitate are plotted in Fig. 7. The several peaks before 500 °C of the DSC profile are accompanied by a large weight loss on the TG curve. They are associated with water loss. The TG curve indicates the complete decomposition of the precursors occurred near 800 °C. Similar DSC/TG curves were obtained for the 0.0%Cr and 1.5%Cr. The wave near 600 °C is due to the initial formation of γ-Al_2O_3, the broad peak centered at 1000 °C may be related to the transition of δ-Al_2O_3 to θ-Al_2O_3 whereas the well-defined peak at 1214 °C corresponds to the transformation of θ-Al_2O_3 to α-Al_2O_3. The DSC/TG curve is in good agreement with the XRD data. During the conventional thermodynamic process, the additional chromium cannot result in more α-Al_2O_3, at least at 1.5%Cr. More details of chromium effect in the sol–gel will be discussed in subsequent works.

Fig. 8 presents the formation of Cr doped Al_2O_3 coatings during the CMAD process and the possible mechanism of γ-Al_2O_3 transformation

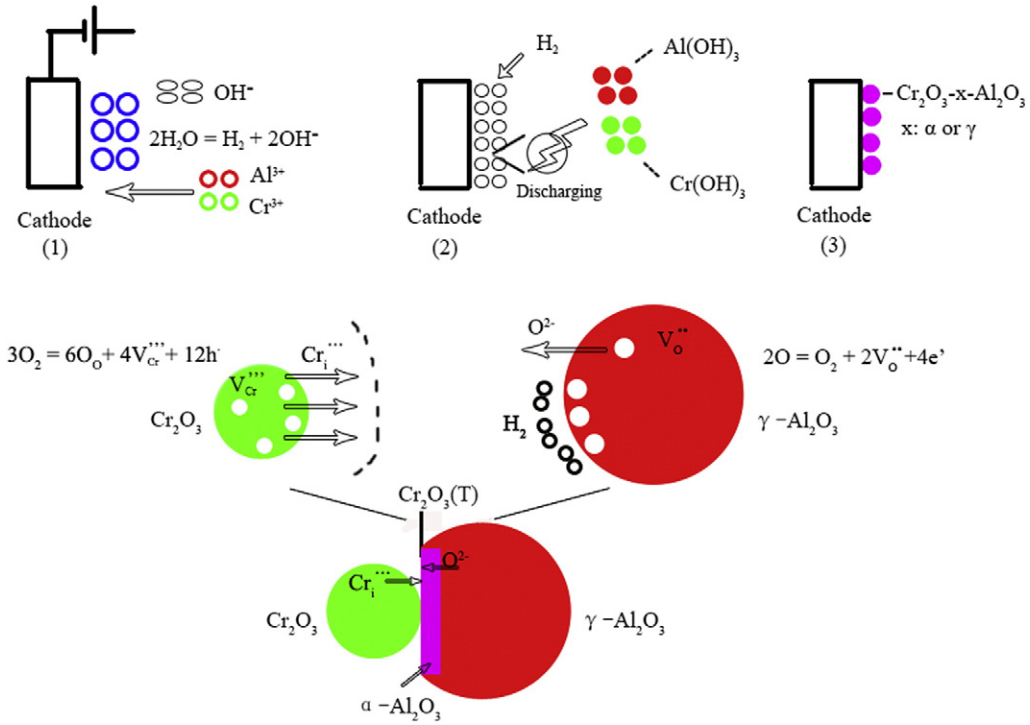

Fig. 8. Schematic illustration of the formation of alumina coatings via CMAD and the possible mechanism of phase change from γ-Al_2O_3 to α-Al_2O_3 with the Cr dopant.

to α-Al_2O_3 induced by the extra Cr content in the electrolyte. In the first step, H_2O was electrically decomposed into H_2 and OH^-, leading to an alkaline environment at the cathode. Meanwhile, the Al^{3+} and Cr^{3+} migrate to the cathode, forming a sol mixture of $Al(OH)_3$ and $Cr(OH)_3$. Then, as most of the voltage drop was on the dense H_2 layer at the interface between the substrate and electrolyte, it began to discharge and created heat. The sol finally formed the composite oxide.

A possible mechanism depicted in Fig. 8 that we define as the 'defect effect' was proposed to explain the transformation process from γ-Al_2O_3 to α-Al_2O_3. Although the coating is mainly a solid solution, it is treated as Cr_2O_3 and γ-Al_2O_3 respectively in the following discussion to make the explanation understandable. In general, Cr_2O_3 is likely to be a p-type semiconductor with defects of $V_{Cr}^{\cdddot{}}$ while γ-Al_2O_3 is an n-type semiconductor with defects of $V_O^{\cdddot{}}$. Taking into account the defect reaction "$2O = O_2 + 2V_O^{\cdddot{}} + 4e'$", the concentration $V_O^{\cdddot{}}$ at the surface of γ-Al_2O_3 increased due to the reducing atmosphere on the cathode, and the concentration rising of $V_O^{\cdddot{}}$ in the γ-Al_2O_3 manifested an external diffusion of O^{2-}. Meanwhile, the concentration of $V_{Cr}^{\cdddot{}}$ rose at the surface of Cr_2O_3 because of the rising concentration of O^{2-} around Cr_2O_3, and it caused an external diffusion of $Cr_i^{\cdddot{}}$. As shown in Fig. 8, there was an inter-diffusion layer of $Cr_i^{\cdddot{}}$ and O^{2-} at the interface between Cr_2O_3 and γ-Al_2O_3, and hence at the leading edge a transient Cr_2O_3 was formed, marked as Cr_2O_3(T) in Fig. 8. As discussed above, we know that the transient Cr_2O_3 was in a localized environment surrounded with many defects. Due to the template effect of Cr_2O_3 and the defects around, the transient Cr_2O_3 at the interface between Cr_2O_3 and γ-Al_2O_3 acted as a nucleation center. With the assistance of energy from plasma discharge and the transient Cr_2O_3 as a nucleation center, the oxygen anion in γ-Al_2O_3 close to Cr_2O_3 (T) is much easier to rearrange and finally completes the transformation from γ-Al_2O_3 to α-Al_2O_3.

Unlike the traditional process of fabricating α-Al_2O_3, the CMAD technique combines the galvanic process with a plasma-chemical reaction. The transitory, high-energy environment created by the plasma can provide a commendable condition for the nucleation of α-Al_2O_3 without serious damage of the substrate. Meanwhile, chromium can enhance the transformation to α-Al_2O_3, which is a promising material for tritium permeation barriers. In short, the CMAD can combine the advantages of an active surface generated by plasma with the available elements found in the doping process. CMAD has great potential for the fabrication of reactor barriers because of its low temperature formation of thermodynamically stable phases of alumina coating on metallic substrate.

4. Conclusions

Cr doped Al_2O_3 ceramic coatings with different Cr concentrations were successfully prepared on 316L stainless steel by a CMAD method. The coatings were composed of Cr doped α-Al_2O_3 and γ-Al_2O_3. The XRD results indicate that the amount of α-Al_2O_3 increased with increasing amount of chromium doped in the electrolyte. The larger amount of α-Al_2O_3 obtained in the coating with Cr doping was because of the 'defect effect', that reduces the activation energy for the anion rearrangement to transform γ-Al_2O_3 to α-Al_2O_3.

Versus the traditional sol–gel process, CMAD shows significant advantages in the formation of α-Al_2O_3. Because of the excellent performance of α-Al_2O_3 at blocking tritium, the Cr doped Al_2O_3 ceramic coatings prepared by CMAD are a promising candidate for tritium barriers.

Acknowledgment

This research was funded by the State Key Laboratory of Surface and Chemistry, China Academy of Engineering Physics (No. SPC 201102), the National Basic Research Program of China (973 Program) under grant No. 2011CB61050, the NSAF program (No. U1430118) and the Chinese National Fusion Project for ITER (No. 2013GB110000).

References

[1] M. Munro, J. Am. Ceram. Soc. 80 (8) (1997) 1919–1928.
[2] A.R. Bunsell, M.H. Berger, J. Eur. Ceram. Soc. 20 (13) (2000) 2249–2260.
[3] G.V. Franks, L. Meagher, Colloids Surf. A Physicochem. Eng. Asp. 214 (1) (2003) 99–110.
[4] G. Zhang, X. Wang, et al., Int. J. Hydrog. Energy 38 (2) (2013) 1157–1165.
[5] W. Krauss, J. Konys, N. Holstein, J. Nucl. Mater. 417 (1) (2011) 1233–1236.
[6] K.S. Forcey, D.K. Ross, C.H. Wu, J. Nucl. Mater. 182 (1991) 36–51.
[7] G.K. Zhang, C.A. Chen, D.L. Luo, et al., Fusion Eng. Des. 87 (7) (2012) 1370–1375.
[8] I. Levin, D. Brandon, J. Am. Ceram. Soc. 81 (8) (1998) 1995–2012.
[9] F.W. Dynys, J.W. Halloran, J. Am. Ceram. Soc. 65 (9) (1982) 442–448.
[10] R.B. Bagwell, G.L. Messing, P.R. Howell, J. Mater. Sci. 36 (7) (2001) 1833–1841.
[11] Y. Wang, C. Suryanarayana, L. An, J. Am. Ceram. Soc. 88 (3) (2005) 780–783.
[12] O. Zywitzki, G. Hoetzsch, F. Fietzke, Surf. Coat. Technol. 82 (1) (1996) 169–175.
[13] R. Brill, F. Koch, J. Mazurelle, Surf. Coat. Technol. 174 (2003) 606–610.
[14] R. Klumpes, C.H.M. Maree, E. Schramm, Mater. Corros. 47 (11) (1996) 619–624.
[15] J. Cai, B. Xu, G. Ling, Appl. Surf. Sci. 268 (2013) 111–116.
[16] K. Okada, A. Hattori, T. Taniguchi, et al., J. Am. Ceram. Soc. 83 (4) (2000) 928–932.
[17] J. Li, Y. Wu, Y. Pan, et al., Ceram. Int. 33 (6) (2007) 919–923.
[18] X. Kong, S. Wang, H. Zhao, et al., Thin Solid Films 518 (15) (2010) 4211–4214.
[19] K.L. Chang, S.C. Chung, S.H. Lai, et al., Appl. Surf. Sci. 236 (1) (2004) 406–415.
[20] Y. Wang, Z. Jiang, X. Liu, et al., Appl. Surf. Sci. 255 (21) (2009) 8836–8840.
[21] B. Henderson, G.F. Imbusch, Optical Spectroscopy of Inorganic Solids, Clarendon Press, Oxford, 1989.
[22] H. Yu, D.R. Clarke, J. Am. Ceram. Soc. 85 (8) (2002) 1966–1970.
[23] L.C. Cossolino, A.R. Zanatta, J. Phys. D. Appl. Phys. 43 (1) (2010) 015302.
[24] X. Chen, L. Liu, Y.Y. Peter, et al., Science 331 (6018) (2011) 746–750.
[25] L. Pach, R. Roy, S. Komarneni, J. Mater. Res. 5 (2) (1990) 278–285.